

Sampling Frequency Thresholds for Quantum Advantage of Quantum Approximate Optimization Algorithm

Danylo Lykov,^{1,2,*} Jonathan Wurtz,^{3,4} Cody Poole,^{5,†} Mark Saffman,^{5,6,‡} Tom Noel,^{7,§} and Yuri Alexeev^{1,¶}

¹Computational Science Division, Argonne National Laboratory, 9700 S. Cass Ave., Lemont, IL 60439, USA

²Department of Computer Science, The University of Chicago, Chicago, IL 60637, USA

³Department of Physics and Astronomy, Tufts University, Medford, MA 02155, USA

⁴QuEra Computing Inc., Boston, MA 02135, USA

⁵Department of Physics, University of Wisconsin - Madison, Madison, WI 53706, USA

⁶ColdQuanta, Inc., 111 N. Fairchild St., Madison, WI 53703, USA

⁷ColdQuanta, Inc., 3030 Sterling Circle, Boulder, CO 80301, USA

In this work, we compare the performance of the Quantum Approximate Optimization Algorithm (QAOA) with state-of-the-art classical solvers such as Gurobi and MQLib to solve the combinatorial optimization problem MaxCut on 3-regular graphs. The goal is to identify under which conditions QAOA can achieve “quantum advantage” over classical algorithms, in terms of both solution quality and time to solution. One might be able to achieve quantum advantage on hundreds of qubits and moderate depth p by sampling the QAOA state at a frequency of order 10 kHz. We observe, however, that classical heuristic solvers are capable of producing high-quality approximate solutions in *linear* time complexity. In order to match this quality for *large* graph sizes N , a quantum device must support depth $p > 11$. Otherwise, we demonstrate that the number of required samples grows exponentially with N , hindering the scalability of QAOA with $p \leq 11$. These results put challenging bounds on achieving quantum advantage for QAOA MaxCut on 3-regular graphs. Other problems, such as different graphs, weighted MaxCut, maximum independent set, and 3-SAT, may be better suited for achieving quantum advantage on near-term quantum devices.

I. INTRODUCTION

Quantum computing promises enormous computational powers that can far outperform any classical computational capabilities [1]. In particular, certain problems can be solved much faster compared with classical computing, as demonstrated experimentally by Google for the task of sampling from a quantum state [2]. Thus, the first important milestone [2] in quantum technology, so-called “quantum supremacy”, was achieved as defined by Preskill [3].

The next milestone, “quantum advantage”, where quantum devices solve *useful* problems faster than classical hardware, is more elusive and has arguably not yet been demonstrated. However, a recent study suggests a possibility of achieving a quantum advantage in runtime over specialized state-of-the-art heuristic algorithms to solve the Maximum Independent Set problem using Rydberg atom arrays [4]. Common classical solutions to several potential applications for near-future quantum computing are heuristic and do not have performance bounds. Thus, proving the advantage of quantum computers is far more challenging [5–7]. Providing an estimate of how quantum advantage over these classical solvers can be achieved is important for the community and is the subject of this paper.

Most of the useful quantum algorithms require large fault-tolerant quantum computers, which remain far in the future. In the near future, however, we can expect to have noisy intermediate-scale quantum (NISQ) devices [8]. In this context variational quantum algorithms (VQAs) show the most promise [9] for the NISQ era, such as the variational quantum eigensolver

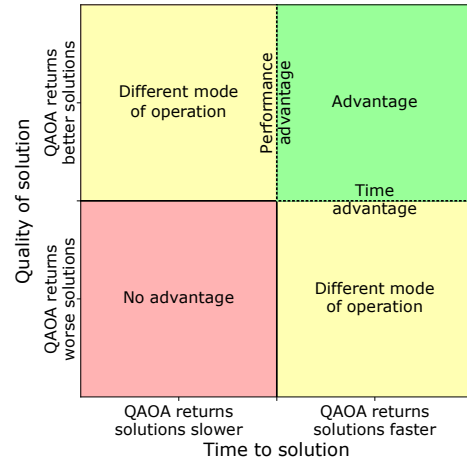


FIG. 1. Locus of quantum advantage over classical algorithms. A particular classical algorithm may return some solution to some ensemble of problems in time T_C (horizontal axis) with some quality C_C (vertical axis). Similarly, a quantum algorithm may return a different solution sampled in time T_Q , which may be faster (right) or slower (left) than classical, with a better (top) or worse (bottom) quality than classical. If QAOA returns better solutions faster than the classical, then there is clear advantage (top right), and conversely no advantage for worse solutions slower than the classical (bottom left).

(VQE) [10] and the Quantum Approximate Optimiza-

tion Algorithm (QAOA) [11]. Researchers have shown remarkable interest in QAOA because it can be used to obtain approximate (i.e., valid but not optimal) solutions to a wide range of useful combinatorial optimization problems [12–14].

In opposition, powerful classical approximate and exact solvers have been developed to find good approximate solutions to combinatorial optimization problems. For example, a recent work by Guerreschi and Matsuura [5] compares the time to solution of QAOA vs. the classical combinatorial optimization suite AKMAXSAT. The classical optimizer takes exponential time with a small prefactor, which leads to the conclusion that QAOA needs hundreds of qubits to be faster than classical. This analysis requires the classical optimizer to find an exact solution, while QAOA yields only approximate solutions. However, modern classical heuristic algorithms are able to return an approximate solution on demand. Allowing for worse-quality solutions makes these solvers extremely fast (on the order of milliseconds), suggesting that QAOA must also be fast to remain competitive. A valid comparison should consider both solution quality and time.

In this way, the locus of quantum advantage has two axes, as shown in Fig. 1: to reach advantage, a quantum algorithm must be both faster and return better solutions than a competing classical algorithm (green, top right). If the quantum version is slower and returns worse solutions (red, bottom left) there is clearly no advantage. However, two more regions are shown in the figure. If the QAOA returns better solutions more slowly than a classical algorithm (yellow, top left), then we can increase the running time for the classical version. It can “try again” and improve its solution with more time. This is a crucial mode to consider when assessing advantage: anytime heuristic algorithms may always outperform quantum algorithms if quantum time to solution is slow. Alternatively, QAOA may return worse solutions faster (yellow, bottom right), which may be useful for time-sensitive applications. In the same way, we may stop the classical algorithm earlier, and the classical solutions will become worse.

One must keep in mind that the reason for using a quantum algorithm is the scaling of its time to solution with the problem size N . Therefore, a strong quantum advantage claim should demonstrate the superior performance of a quantum algorithm in the large- N limit.

This paper focuses on the MaxCut combinatorial optimization problem on 3-regular graphs for various problem size N . MaxCut is a popular benchmarking problem for QAOA because of its simplicity and straightforward implementation. We propose a fast “fixed-angle” approach to running QAOA that speeds up QAOA while preserving solution quality compared with slower conventional approaches. We evaluate the expectation value of noiseless QAOA solution quality using tensor network simulations on classical hardware. We then find the time required for classical solvers to match this expected QAOA solution quality. Surprisingly, we observe that even for the small-

est possible time, the classical solution quality is above our QAOA solution quality for $p = 11$, our largest p with known performance. Therefore, we compensate for this difference in quality by using multishot QAOA and find the number of samples K required to match the classical solution quality. K allows us to characterize quantum device parameters, such as sampling frequency, required for the quantum algorithm to match the classical solution quality.

The following sections outline the solution quality bounds for fixed-angle QAOA and the challenges in competing against today’s classical optimizers. Section II outlines the methodology for the comparison and configuration of the classical solvers used in the work. Section III outlines the performance of fixed-angle QAOA, in terms of both performance and time to solution. For comparison, Section IV outlines the performance of the classical optimizers used in this work. Section V discusses the requirements for QAOA, and Section VI concludes with an outlook on the goal of quantum advantage with QAOA.

II. METHODOLOGY

Both classical solvers and QAOA return a bitstring as a solution to the MaxCut problem. To compare the algorithms, we must decide on a metric to use to measure the quality of the solution. A common metric for QAOA and many classical algorithms is the approximation ratio, which is defined as the ratio of cut value (as defined in Eq. (2)) of the solution divided by the optimal (i.e., maximum possible) cut value for the given graph. This metric is hard to evaluate heuristically for large N , since we do not know the optimal solution. We therefore use the cut fraction as the metric for solution quality, which is the cut value divided by the number of edges.

We analyze the algorithms on an ensemble of problem instances. Some instances may give advantage, while others may not. We therefore analyze ensemble advantage, which compares the average solution quality over the ensemble. The set of 3-regular graphs is extremely large for large graph size N , so for classical heuristic algorithms we evaluate the performance on a subset of graphs. We then look at the mean of the cut fraction over the ensemble, which is the statistical approximation of the mean of the cut fraction over all 3-regular graphs.

A. QAOA Methodology

Usually QAOA is thought of as a hybrid algorithm, where a quantum-classical outer loop optimizes the angles γ, β through repeated query to the quantum device by a classical optimizer. Depending on the noise, this process may require hundreds or thousands of queries in order to find optimal angles, which slows the computation. To our knowledge, no comprehensive work exists on exactly how many queries may be required to find

such angles. It has been numerically observed [6; 15], however, that for small graph size $N = 12$ and $p = 4$, classical noise-free optimizers may find good angles in approximately 100 steps, which can be larger for higher N and p . Each step may need order 10^3 bitstring queries to average out shot noise and find expectation values for an optimizer, and thus seeking global angles may require approximately 100 000 queries to the simulator. The angles are then used for preparing an ansatz state, which is in turn measured (potentially multiple times) to obtain a solution. Assuming a sampling rate of 1 kHz, this approach implies a QAOA solution of approximately 100 seconds.

Recent results, however, suggest that angles may be precomputed on a classical device [16] or transferred from other similar graphs [17]. Going a step further, a recent work finds that evaluating regular graphs at particular fixed angles has good performance on all problem instances [18]. These precomputed or fixed angles allow the outer loop to be bypassed, finding close to optimal results in a single shot. In this way, a 1000 Hz QAOA solution can be found in milliseconds, a speedup of several orders of magnitude.

For this reason we study the prospect for quantum advantage in the context of fixed-angle QAOA. For d -regular graphs, there exist particular fixed angles with universally good performance [19]. Additionally, as will be shown in Section III D, one can reasonably expect that sampling a single bitstring from the fixed-angle QAOA will yield a solution with a cut fraction close to the expectation value.

The crucial property of the fixed-angle single-shot approach is that it is guaranteed to work for any graph size N . On the other hand, angle optimisation could be less productive for large N , and the multiple-shot (measuring the QAOA ansatz multiple times) approach *is* less productive for large N , as shown in Section III E. Moreover, the quality of the solution scales with depth as \sqrt{p} [19], which is faster than with the number of samples $\sqrt{\log K}$, instructing us to resort to multishot QAOA only if larger p is unreachable. Thus, the fixed-angle single-shot QAOA can robustly speed up finding a good approximate solution from the order of seconds to milliseconds, a necessity for advantage over state-of-the-art anytime heuristic classical solvers, which can get good or exact solutions in approximately milliseconds. Crucially, single-shot QAOA quality of solution can be maintained for all sizes N at fixed depth p , which can mean constant time scaling, for particularly capable quantum devices.

To simulate the expectation value of the cost function for QAOA, we employ a classical quantum circuit simulation algorithm QTensor [20–22]. This algorithm is based on tensor network contraction and is described in more detail in Appendix A. Using this approach, one can simulate expectation values on a classical computer even for circuits with millions of qubits.

B. Classical Solvers

Two main types of classical MaxCut algorithms exist: approximate algorithms and heuristic solvers. Approximate algorithms guarantee a certain quality of solution for any problem instance. Such algorithms [23; 24] also provide polynomial-time scaling. Heuristic solvers [25; 26] are usually based on branch-and-bound methods [27] that use heuristic rules for branch pruning. These heuristics are usually designed to run well on graphs that are common in practical use cases. Heuristic solvers typically return better solutions than do approximate solvers, but they provide no guarantee on the quality of the solution.

The comparison of QAOA with classical solvers thus requires making choices of measures that depend on the context of comparison. From a theory point of view, guaranteed performance is more important; in contrast, from an applied point of view, heuristic performance is the measure of choice. A previous work [18] demonstrates that QAOA provides better performance guarantees than does the Goemans–Williamson algorithm [24]. In this paper we compare against heuristic algorithms since such a comparison is more relevant for real-world problems. On the other hand, the performance of classical solvers reported in this paper can depend on a particular problem instance.

We evaluate two classical algorithms using a single node of Argonne’s Skylake testbed; the processor used is an Intel Xeon Platinum 8180M CPU @ 2.50 GHz with 768 GB of RAM.

The first algorithm we study is the Gurobi solver [25], which is a combination of many heuristic algorithms. We evaluate Gurobi with an improved configuration based on communication with Gurobi support [28]. We use `Symmetry=0` and `PreQLinearize=2` in our improved configuration. As further tweaks and hardware resources may increase the speed, the results here serve as a characteristic lower bound on Gurobi performance rather than a true guarantee. We run Gurobi on 100 random-regular graphs for each size N and allow each optimization to run for 30 minutes. During the algorithm runtime we collect information about the process, in particular the quality of the best-known solution. In this way we obtain a “performance profile” of the algorithm that shows the relation between the solution quality and the running time. An example of such a performance profile for $N = 256$ is shown in Fig. 4. Gurobi was configured to use only a single CPU, to avoid interference in runtime between different Gurobi optimization runs for different problem instances. In order to speed up collection of the statistics, 55 problem instances were executed in parallel.

The second algorithm is MQLib [26], which is implemented in C++ and uses a variety of different heuristics for solving MaxCut and QUBO problems. We chose the BURER2002 heuristic since in our experiments it performs the best for MaxCut on random regular graphs. Despite using a single thread, this algorithm is much faster than Gurobi; thus we run it for 1 second. In the

same way as with Gurobi, we collect the “performance profile” of this algorithm.

While QAOA and Gurobi can be used as general-purpose combinatorial optimization algorithms, this algorithm is designed to solve MaxCut problems only, and the heuristic was picked that demonstrated the best performance on the graphs we considered. In this way we use Gurobi as a “worst-case” classical solver, which is capable of solving the same problems as QAOA can. Moreover, Gurobi is a well-established commercial tool that is widely used in industry. Note, however, that we use QAOA fixed angles that are optimized specifically for 3-regular graphs, and one can argue that our fixed-angle QAOA is an algorithm designed for 3-regular MaxCut. For this reason we also consider the “best-case” MQLib+BURER2002 classical algorithm, which is designed for MaxCut, and we choose the heuristic that performs best on 3-regular graphs.

III. QAOA PERFORMANCE

Two aspects are involved in comparing the performance of algorithms, as outlined in Fig. 1: time to solution and quality of solution. In this section we evaluate the performance of single-shot fixed-angle QAOA. As discussed in the introduction, the time to solution is a crucial part and for QAOA is dependent on the initialization time and the number of rounds of sampling. Single-shot fixed-angle QAOA involves only a single round of sampling, and so the time to solution can be extremely fast, with initialization time potentially becoming the limiting factor. This initialization time is bound by the speed of classical computers, which perform calibration and device control. Naturally, if one is able to achieve greater initialization speed by using better classical computers, the same computers can be used to improve the speed of solving MaxCut classically. Therefore, it is also important to consider the time scaling of both quantum initialization and classical runtime.

The quality of the QAOA solution is the other part of performance. The discussion below evaluates this feature by using subgraph decompositions and QAOA typicality, including a justification of single-shot sampling.

A. QAOA Introduction

QAOA is a variational ansatz algorithm structured to provide solutions to combinatorial optimization problems. The ansatz is constructed as p repeated applications of an objective \hat{C} and mixing \hat{B} unitary:

$$|\gamma, \beta\rangle = e^{-i\beta_p \hat{B}} e^{-i\gamma_p \hat{C}} (\dots) e^{-i\beta_1 \hat{B}} e^{-i\gamma_1 \hat{C}} |+\rangle, \quad (1)$$

where \hat{B} is a sum over Pauli X operators $\hat{B} = \sum_i^N \hat{\sigma}_x^i$. A common problem instance is MaxCut, which strives to bipartition the vertices of some graph \mathcal{G} such that the

maximum number of edges have vertices in opposite sets. Each such edge is considered to be “cut” by the bipartition. This may be captured in the objective function

$$\hat{C} = \frac{1}{2} \sum_{\langle ij \rangle \in \mathcal{G}} (1 - \hat{\sigma}_z^i \hat{\sigma}_z^j), \quad (2)$$

whose eigenstates are bipartitions in the Z basis, with eigenvalues that count the number of cut edges. To get the solution to the optimization problem, one prepares the ansatz state $|\vec{\gamma}, \vec{\beta}\rangle$ on a quantum device and then measures the state. The measured bitstring is the solution output from the algorithm.

While QAOA is guaranteed to converge to the exact solution in the $p \rightarrow \infty$ limit in accordance with the adiabatic theorem [11; 29], today’s hardware is limited to low depths $p \sim 1$ to 5, because of the noise and decoherence effects inherent to the NISQ era.

B. Subgraph Decomposition

A useful tool for analyzing the performance of QAOA is the fact that QAOA is local [11; 13]: the entanglement between any two qubits at a distance of $\geq 2p$ steps from each other is strictly zero. For a similar reason, the expectation value of a particular edge $\langle ij \rangle$

$$f_{\langle ij \rangle} = \frac{1}{2} \langle \vec{\gamma}, \vec{\beta} | 1 - \hat{\sigma}_z^i \hat{\sigma}_z^j | \vec{\gamma}, \vec{\beta} \rangle \quad (3)$$

depends only on the structure of the graph within p steps of edge $\langle ij \rangle$. Regular graphs have a finite number of such local structures (also known as subgraphs) [18], and so the expectation value of the objective function can be rewritten as a sum over subgraphs

$$\langle \hat{C} \rangle = \sum_{\text{subgraphs } \lambda} M_\lambda(\mathcal{G}) f_\lambda. \quad (4)$$

Here, λ indexes the different possible subgraphs of depth p for a d regular graph, $M_\lambda(\mathcal{G})$ counts the number of each subgraph λ for a particular graph \mathcal{G} , and f_λ is the expectation value of the subgraph (e.g., Eq. (3)). For example, if there are no cycles $\leq 2p + 1$, only one subgraph (the “tree” subgraph) contributes to the sum.

With this tool we may ask and answer the following question: What is the typical performance of single-shot fixed-angle QAOA, evaluated over some ensemble of graphs? Here, performance is characterized as the typical (average) fraction of edges cut by a bitstring solution returned by a single sample of fixed-angle QAOA, averaged over all graphs in the particular ensemble.

For our study we choose the ensemble of 3-regular graphs on N vertices. Different ensembles, characterized by different connectivity d and size N , may have different QAOA performance [30; 31].

Using the structure of the random regular graphs, we can put bounds on the cut fraction by bounding the number of different subgraphs and evaluating the number of large cycles. These bounds become tighter for $N \rightarrow \infty$ and fixed p since the majority of subgraphs become trees and 1-cycle graphs. We describe this analysis in detail in Appendix C, which shows that the QAOA cut fraction will equal the expectation value on the “tree” subgraph, which may be used as a “with high probability” (WHP) proxy of performance. Furthermore, using a subgraph counting argument, we may count the number of tree subgraphs to find an upper and lower WHP bound on the cut fraction for smaller graphs. These bounds are shown as the boundaries of the red and green regions in Fig. 2.

C. Ensemble Estimates

A more straightforward but less rigorous characterization of QAOA performance is simply to evaluate fixed-angle QAOA on a subsample of graphs in the ensemble. The results of such an analysis require an assumption not on the particular combinatorial graph structure of ensembles but instead on the typicality of expectation values on subgraphs. This is an assumption on the structure of QAOA and allows an extension of typical cut fractions from the large N limit where most subgraphs are trees to a small N limit where typically a very small fraction of subgraphs are trees.

Figure 2 plots the ensemble-averaged cut fraction for $p = 2$ and various sizes of graphs. For $N \leq 16$, the ensemble includes every 3-regular graph (4,681 in total). For each size of $N > 16$, we evaluate fixed-angle QAOA on 1,000 3-regular graphs drawn at random from the ensemble of all 3-regular graphs for each size $N \in (16, 256]$. Note that because the evaluation is done at fixed angles, it may be done with minimal quantum calculation by a decomposition into subgraphs, then looking up the subgraph expectation value f_λ from [18]. This approach is also described in more detail in [32]. In this way, expectation values can be computed as fast as an isomorphism check.

From Fig. 2 we observe that the median cut fraction across the ensemble appears to concentrate around that of the tree subgraph value, even for ensembles where the typical graph is too small to include many tree subgraphs. Additionally, the variance (dark fill) reduces as N increases, consistent with the fact that for larger N there are fewer kinds of subgraphs. Furthermore, the absolute range (light fill), which plots the largest and smallest expectation value across the ensemble, is consistently small. While the data for the absolute range exists here only for $N \leq 16$ because of complete sampling of the ensemble, one can reasonably expect that these absolute ranges extend for all N , suggesting that the absolute best performance of $p = 2$ QAOA on 3-regular graphs is around ≈ 0.8 .

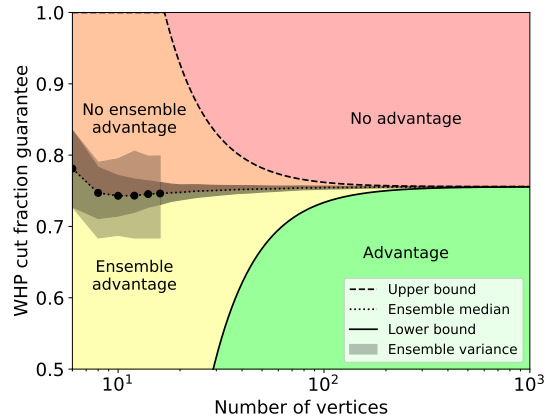


FIG. 2. $p = 2$ QAOA cut fraction guarantees under different assumptions. Dashed and solid lines plot with high probability the lower and upper bounds on cut fractions, respectively, assuming only graph theoretic typicality on the number of subgraphs. Dotted plots are the ensemble median over an ensemble of 3-regular graphs; for $N \leq 16$ (dots); this includes all graphs, while for $N > 16$ this is an ensemble of 1,000 graphs for each size. We used 32 sizes between 16 and 256. Dark black fill plots the variance in the cut fraction over the ensemble, and light black fill plots the extremal values over the ensemble. The median serves as a proxy of performance assuming QAOA typicality. Given a particular cut from a classical solver, there may be different regions of advantage, shown by the four colors and discussed in the text.

We numerically observe across a range of p (not shown) that these behaviors persist: the typical cut fraction is approximately equal to that of the tree subgraph value $f_{p\text{-tree}}$ even in the limit where no subgraph is a tree. This suggests that the typical subgraph expectation value $f_\lambda \approx f_{p\text{-tree}}$, and only an atypical number of subgraphs have expectation values that diverge from the tree value. A heuristic example is shown in Table I, which indicates that the expectation value of large single-loop graphs is close to the tree value. With this observation, we may use the value $f_{p\text{-tree}}$ as a proxy for the average cut fraction of fixed-angle QAOA.

These analyses yield four different regimes for advantage vs. classical algorithms, shown in Fig. 2. If a classical algorithm yields small cut fractions for large graphs (green, bottom right), then there is advantage in a strong sense. Based only on graph combinatorics, with high probability most of the edges participate in few cycles, and thus the cut fraction is almost guaranteed to be around the tree value, larger than the classical solver. Conversely, if the classical algorithm yields large cut fractions for large graphs (red, top right), there is no advantage in the strong sense: QAOA will yield, for example, only ~ 0.756 for $p = 2$ because most edges see no global structure. This analysis emphasizes that of [13], which

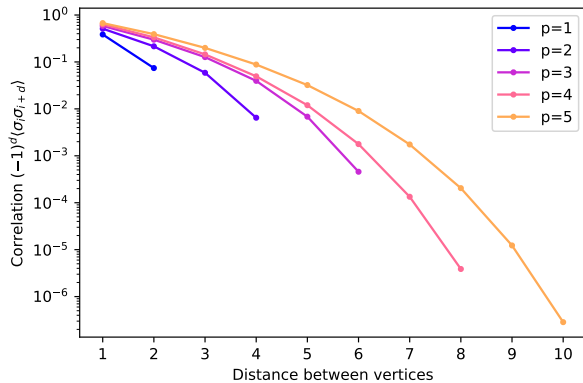


FIG. 3. Long-range antiferromagnetic correlation coefficient on the 3-regular Bethe lattice, which is a proxy for an $N \rightarrow \infty$ typical 3-regular graph. Horizontal indexes the distance between two vertices. QAOA is strictly local, which implies that no correlations exist between vertices a distance $> 2p$ away. As shown here, however, these correlations are exponentially decaying with distance. This suggests that even if the QAOA “sees the whole graph,” one can use the central limit theorem to argue that the distribution of QAOA performance is Gaussian with the standard deviation of $\propto 1/\sqrt{N}$.

suggests that QAOA needs to “see” the whole graph in order to get reasonable performance.

Two additional performance regimes for small graphs exist, where QAOA can reasonably “see” the whole graph. If a classical algorithm yields small cut fractions for small graphs (yellow, bottom left), then there is advantage in a weak sense, which we call the “ensemble advantage.” Based on QAOA concentration, there is at least a 50% chance that the QAOA result on a particular graph will yield a better cut fraction than will the classical algorithm; assuming that the variance in cut fraction is small, this is a “with high probability” statement. Conversely, if the classical algorithm yields large cut fractions for small graphs (orange, top left), there is no advantage in a weak sense. Assuming QAOA concentration, the cut fraction will be smaller than the classical value, and for some classical cut fraction there are no graphs with advantage (e.g., > 0.8 for $p = 2$).

Based on these numerical results, we may use the expectation value of the tree subgraph $f_{p\text{-tree}}$ as a high-probability proxy for typical fixed-angle QAOA performance on regular graphs. For large N , this result is validated by graph-theoretic bounds counting the typical number of tree subgraphs in a typical graph. For small N , this result is validated by fixed-angle QAOA evaluation on a large ensemble of graphs.

D. Single-shot Sampling

A crucial element of single-shot fixed-angle QAOA is that the typical bitstring measured from the QAOA

ansatz has a cut value similar to the average. This fact was originally observed by Farhi et al. in the original QAOA proposal [11]: because of the strict locality of QAOA, vertices a distance more than $> 2p$ steps from each other have a ZZ correlation of strictly zero. Thus, for large graphs with a width $> 2p$, by the central limit theorem the cut fraction concentrates to a Gaussian with a standard deviation of order $\frac{1}{\sqrt{N}}$ around the mean. If the distribution is Gaussian, then by definition there is a 50% chance of measuring a value greater than the average and a vanishing chance of measuring a value less than a few standard deviations below the mean. As the variance grows sublinearly in N , the values concentrate at the mean, and thus with high probability measuring a single sample of QAOA will yield a solution with a cut value close to the average.

However, this result is limited in scope for larger depths p , because it imposes no requirements on the strength of correlations for vertices within distance $\leq 2p$. Therefore, here we strengthen the argument of Farhi et al. and show that these concentration results may persist even in the limit of large depth p and small graphs N . We formalize these results by evaluating the ZZ correlations of vertices within $2p$ steps, as shown in Fig. 3. Expectation values are computed on the 3-regular Bethe lattice, which has no cycles and thus can be considered the $N \rightarrow \infty$ typical limit. Instead of computing the nearest-neighbor correlation function, the x-axis computes the correlation function between vertices a certain distance apart. For distance 1, the correlations are that of the objective function $f_{p\text{-tree}}$. Additionally, for distance $> 2p$, the correlations are strictly zero in accordance with the strict locality of QAOA. For distance $\leq 2p$, the correlations are exponentially decaying with distance. Consequently, even for vertices within the lightcone of QAOA, the correlation is small; and so by the central limit theorem the distribution will be Gaussian.

Unfortunately, this result strictly holds only for graphs that have no cycles $\leq 2p + 1$. However, we can reasonably extend the argument of Section III C on typicality of subgraph expectation values. Under this typicality argument, the correlations between close vertices is still exponentially decaying with distance, even though the subgraph may not be a tree and there are multiple short paths between vertices. Thus, for all graphs, by the central limit theorem the distribution of solutions concentrates as a Gaussian with a standard deviation of order $\frac{1}{\sqrt{N}}$ around the mean. By extension, with probability $\sim 50\%$, any single measurement will yield a bitstring with a cut value greater than the average. These results of cut distributions have been found heuristically in [33].

The results are a full characterization of the fixed-angle single-shot QAOA on 3-regular graphs. Given a typical graph sampled from the ensemble of all regular graphs, the typical cut fraction from level p QAOA will be about that of the expectation value of the p -tree $f_{p\text{-tree}}$. The distribution of bitstrings is concentrated as a Gaussian of

subextensive variance around the mean, indicating that one can find a solution with quality greater than the mean with order 1 samples. Furthermore, because the fixed angles bypass the hybrid optimization loop, the number of queries to the quantum simulator is reduced by orders of magnitude, yielding solutions on potentially millisecond timescales.

E. Multiple shot Sampling

In the preceding section we demonstrated that the variance of MaxCut cost distribution falls as $1/\sqrt{N}$, which deems impractical the usage of multiple shots for large graphs. However, it is worth verifying more precisely the effect of variance on the QAOA performance. The multiple-shot QAOA involves measuring the bitstring from the same ansatz state and then picking the bitstring with the best cost. To evaluate such an approach, we need to find the expectation value for the best bitstring over K measurements.

As shown above, the distribution of cost for each measured bitstring is Gaussian, $p(x) = G(\frac{x-\mu_p}{\sigma_N})$. The probability density function for the best of K bitstrings ξ is

$$p_N(\xi) = \frac{d}{d\xi} F_K(\xi) = \frac{d}{d\xi} F_1^K(\xi) = K F^{K-1}(\xi) p(\xi), \quad (5)$$

Where $F_1(\xi)$ is a cumulative distribution function for the Gaussian variable: $F_1(\xi) = \int_{-\infty}^{\xi} p(x) dx$. The expectation value for ξ can be found by $E_K = \int_{-\infty}^{\infty} dx x p_N(x)$. While the analytical expression for the integral can be extensive, a good upper bound exists for it: $E_K \leq \sigma\sqrt{2 \log K} + \mu$.

Combined with the $1/\sqrt{N}$ scaling of the standard deviation, we can obtain a bound on improvement in cut fraction from sampling K times:

$$\Delta = \gamma_p \sqrt{\frac{2}{N} \log K}, \quad (6)$$

where γ_p is a scaling parameter. The value Δ is the difference of solution quality for multishot and single-shot QAOA. Essentially it determines the utility of using multishot QAOA. We can determine the scaling constant γ_p by classically simulating the distribution of the cost value in the ansatz state. We perform these simulations using QTensor for an ensemble of graphs with $N \leq 26$ to obtain $\gamma_6 = 0.1926$ and $\gamma_{11} = 0.1284$.

It is also worthwhile to verify the $1/\sqrt{N}$ scaling, by calculating γ_p for various N . We can do so for smaller $p = 3$ and graph sizes $N \leq 256$. We calculate the standard deviation by $\Delta C = \sqrt{\langle C^2 \rangle - \langle C \rangle^2}$ and evaluate the $\langle C^2 \rangle$ using QTensor. This evaluation gives large light cones for large p ; the largest that we were able to simulate is $p = 3$. From the deviations ΔC we can obtain values for γ_3 . We find that for all N the values stay within 5% of average over all N . This shows that they do not depend

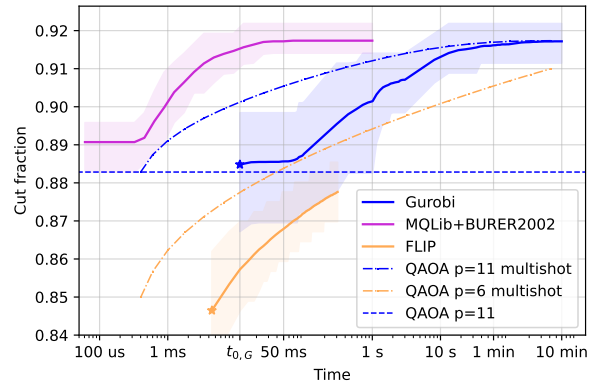


FIG. 4. Evolution of cut fraction value in the process of running the classical algorithms solving 3-regular MaxCut with $N=256$. The shaded area shows 90-10 percentiles interval, and the solid line shows the mean cut fraction over 100 graphs. The dashed lines show the expectation value of single-shot QAOA for $p = 6, 11$, and the dash-dotted lines show the expected performance for multishot QAOA given a sampling rate of 5 kHz. Note that for this $N = 256$ the multi-shot QAOA with $p = 6$ can compete with Gurobi at 50 milliseconds. However, the slope of the multi-shot line will decrease for larger N , reducing the utility of the multi-shot QAOA.

on N , which in turn signifies that the $1/\sqrt{N}$ scaling is a valid model.

To compare multishot QAOA with classical solvers, we plot the expected performance of multishot QAOA in Fig. 4 as dash-dotted lines. We assume that a quantum device is able to sample at the 5kHz rate. Today’s hardware is able to run up to $p = 5$ and achieve the 5 kHz sampling rate [34].

For small N , reasonable improvement can be achieved by using a few samples. For example, for $N = 256$ with $p = 6$ and just $K = 200$ shots, QAOA can perform as well as single-shot $p = 11$ QAOA. For large N , however, too many samples are required to obtain substantial improvement for multishot QAOA to be practical.

IV. CLASSICAL PERFORMANCE

To compare the QAOA algorithm with its classical counterparts, we choose the state-of-the art algorithms that solve the similar spectrum of problems as QAOA, and we evaluate the time to solution and solution quality. Here, we compare two algorithms: Gurobi and MQLib+BURER2002. Both are anytime heuristic algorithms that can provide an approximate solution at arbitrary time. For these algorithms we collect the “performance profiles”—the dependence of solution quality on time spent finding the solution. We also evaluate performance of a simple MaxCut algorithm FLIP. This algorithm has a proven linear time scaling with input size.

A. Gurobi Solver

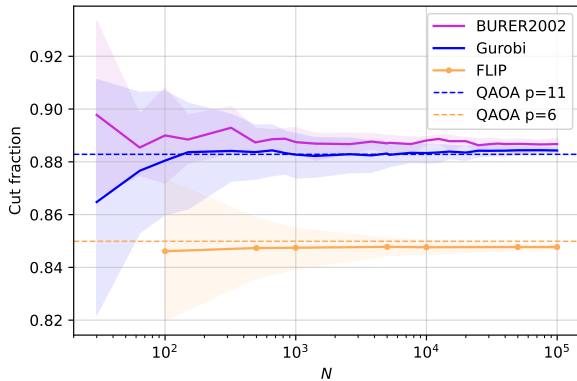


FIG. 5. Zero-time performance for graphs of different size N . The Y-value is the cut fraction obtained by running corresponding algorithms for minimum possible time. This corresponds to the Y-value of the star marker in Fig. 4. Dashed lines show the expected QAOA performance for $p = 11$ (blue) and $p = 6$ (yellow). QAOA can outperform the FLIP algorithm at depth $p > 6$, while for Gurobi it needs $p > 11$. Note that in order to claim advantage, QAOA has to provide the zero-time solutions in faster time than FLIP or Gurobi does. These times are shown on Fig. 6.

It returns a single solution after a short time. To obtain a better FLIP solution, one may run the algorithm several times and take the best solution, similarly to the multishot QAOA.

Both algorithms have to read the input and perform some initialization step to output any solution. This initialization step determines the minimum time required for getting the initial solution—a “first guess” of the algorithm. This time is the leftmost point of the performance profile marked with a star in Fig. 4. We call this time t_0 and the corresponding solution quality zero-time performance.

We observe two important results.

1. Zero-time performance is constant with N and is comparable to that of $p = 11$ QAOA, as shown in Fig. 5, where solid lines show classical performance and dashed lines show QAOA performance.
2. t_0 scales as a low-degree polynomial in N , as shown in Fig. 6. The y-axis is t_0 for several classical algorithms.

Since the zero-time performance is slightly above the expected QAOA performance at $p = 11$, we focus on analyzing this “zero-time regime.” In the following subsections we discuss the performance of the classical algorithms and then proceed to the comparison with QAOA.

In our classical experiments, as mentioned in Section II B, we collect the solution quality with respect to time for multiple N and graph instances. An example averaged solution quality evolution is shown in Fig. 4 for an ensemble of 256 vertex 3-regular graphs. Between times 0 and $t_{0,G}$, the Gurobi algorithm goes through some initialization and quickly finds some naive approximate solution. Next, the first incumbent solution is generated, which will be improved in further runtime. Notably, for the first 50 milliseconds, no significant improvement to solution quality is found. After that, the solution quality starts to rise and slowly converge to the optimal value of ~ 0.92 .

Additionally, Gurobi estimates the upper bound for the optimal cost, indicated by the purple line. When the upper bound and the cost for incumbent solution match, the optimal solution is found.

Notably, the x-axis of Fig. 4 is logarithmic: the lower and upper bounds eventually converge after exponential time with a small prefactor, ending the program and yielding the exact solution. Additionally, the typical upper and lower bounds of the cut fraction of the best solution are close to 1. Even after approximately 10 seconds for a 256-vertex graph, the algorithm returns cut fractions with very high quality ~ 0.92 , far better than intermediate-depth QAOA.

The zero-time performance of Gurobi for $N = 256$ corresponds to the Y-value of the star marker on Fig. 4. We plot this value for various N in Fig. 5. As shown in the figure, zero-time performance goes up and reaches a constant value of ~ 0.882 at $N \sim 100$. Even for large graphs of $N = 10^5$, the solution quality stays at the same level.

Such solution quality is returned after time $t_{0,G}$, which we plot in Fig. 6 for various N . For example, for a 1000-node graph it will take ~ 40 milliseconds to return the first solution. Evidently, this time scales as a low-degree polynomial with N . This shows that Gurobi can consistently return solutions of quality ~ 0.882 in polynomial time.

B. MQLib+BURER2002 and FLIP Algorithms

The MQLib algorithm with the BURER2002 heuristic shows significantly better performance, which is expected since it is specific to MaxCut. As shown in Fig. 4 for $N = 256$ and in Fig. 6 for various N , the speed of this algorithm is much better compared with Gurobi’s. Moreover, t_0 for MQLib also scales as a low-degree polynomial, and for 1,000 nodes MQLib can return a solution in 2 milliseconds. The zero-time performance shows the same constant behavior, and the value of the constant is slightly higher than that of Gurobi, as shown in Fig. 5.

While for Gurobi and MQLib we find the time scaling heuristically, the FLIP algorithm is known to have linear time scaling. With our implementation in Python, it

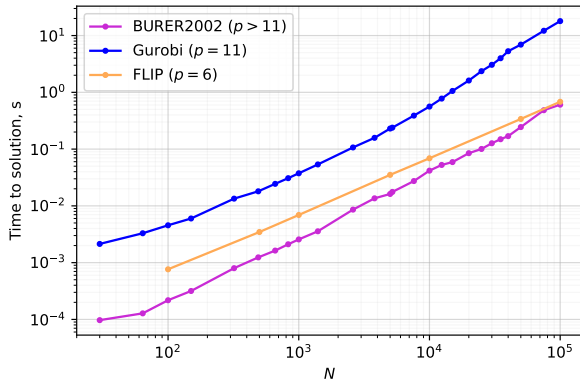


FIG. 6. Time required for a single-shot QAOA to match classical MaxCut algorithms. The blue line shows time for comparing with the Gurobi solver and using $p = 11$; the yellow line shows comparison with the FLIP algorithm and $p = 6$. Each quantum device that runs MaxCut QAOA can be represented on this plot as a point, where the x-axis is the number of qubits and the y-axis is the time to solution. For any QAOA depth p , the quantum device should return at least one bitstring faster than the Y-value on this plot.

shows speed comparable to that of MQLib and solution quality comparable to QAOA $p = 6$. We use this algorithm as a demonstration that a linear-time algorithm can give constant performance for large N , averaged over multiple graph instances.

V. RESULTS AND DISCUSSION

In the preceding sections we analyzed the performance of classical and quantum algorithms for solving MaxCut on 3-regular graphs. In Section III we find that one can put limits on the QAOA MaxCut performance even when the exact structure of a 3-regular graph is unknown using fixed angles. In a general case, any optimizer will find good parameters $\vec{\gamma}, \vec{\beta}$ that give close to an optimal solution on any 3-regular graph. However, trying to optimize the parameters $\vec{\gamma}, \vec{\beta}$ for a particular graph instance may not provide significant improvement in solution quality and comes at the expense of sampling the state thousands of times, slowing convergence. We therefore focus on the “fixed-angle” regime and evaluate the performance of QAOA at these fixed angles. We have shown that for large N the average cut fraction for QAOA solutions on 3-regular graphs converges to a fixed value f_{tree} . If memory limitations permit, we evaluate these values numerically using tensor network simulations. This gives us the average QAOA performance for any large N and $p \leq 11$. To further strengthen the study of QAOA performance estimations, we verify that for the small N , the performance is close to the same value f_{tree} . We are able to numerically verify that for $p \leq 4$ and small N the typical

cut fraction is close to f_{tree} , as shown on Fig. 2.

Combining the large- N theoretical analysis and small- N heuristic evidence, we are able to predict the average performance of QAOA on 3-regular graphs for $p \leq 11$. We note that today’s hardware can run QAOA up to $p \leq 4$ [12] and that for larger depths the hardware noise prevents achieving better QAOA performance. Therefore, the $p \leq 11$ constraint is not an important limitation for our analysis.

Having calculated the performance of QAOA, we experimentally evaluate the performance of classical solvers. We observe that the zero-time performance, which is the quality of the fastest classical solution, is above the expected quality of QAOA $p = 11$, as shown in Fig. 5. To compete with classical solvers, QAOA has to return better solutions.

To improve the performance of QAOA, one can sample many bitstrings and then take the best one. This approach will work only if the variance of the cut fraction distribution is large, however. For example, if the variance is zero, measuring the ansatz state would return only bitstrings with a fixed cut value. By analyzing the correlations between the qubits in Section III, we show that the distribution of the cut fraction is a Gaussian with the variance on the order of $1/\sqrt{N}$. The expectation value of maximum of K samples is proportional to the variance, as shown in Equation 6. This equation determines the performance of multishot QAOA. In the large N limit the variance is small, and one might need to measure more samples in order to match the classical performance.

If we have the mean performance of a classical algorithm, we can estimate the number of samples K required for QAOA to match the classical performance. It is important to explain the difference between classical and quantum expected cut fraction as $\Delta_p(t)$, which is a function of the running time of the classical algorithm. Moreover, it also depends on p , since p determines QAOA expected performance. If $\Delta_p(t) < 0$, the performance of QAOA is better, and we need only a $K = 1$ sample. In order to provide an advantage, QAOA would have to measure this sample faster than the classical algorithm, as per Fig. 1. On the other hand, if $\Delta_p(t) > 0$, the classical expectation value is larger than the quantum one, and we have to perform multisample QAOA. We can find K by inverting Equation 6. In order to match the classical algorithm, a quantum device should be able to run these K samples in no longer than t . We can therefore get the threshold sampling frequency.

$$\nu_p(t) = \frac{K}{t} = \frac{1}{t} \exp\left(\frac{N}{\gamma_p^2} \Delta_p(t)^2\right) \quad (7)$$

The scaling of $\Delta_p(t)$ with t is essential here since it determines at which point t we will have the smallest sampling frequency for advantage. We find that for BURER2002, the value of $\Delta(t)$ is the lowest for the smallest possible $t = t_0$, which is when a classical algorithm can produce its first solution.

Time t_0 is shown on Fig. 6 for different classical algorithms. We note that in the figure the time scales polynomially with the number of nodes N . Figure 5 shows the mean cut fraction for the same classical algorithms, as well as the expectation value of QAOA at $p = 6, 11$. These two figures show that a simple linear-runtime FLIP algorithm is fast and gives a performance on par with $p = 6$ QAOA. In this case $\Delta_6(t_0) < 0$, and we need to sample only a single bitstring. To obtain the $p = 6$ sampling frequency for advantage over the FLIP algorithm, one has to invert the time from Fig. 6. If the quantum device is not capable of running $p = 6$ with little noise, the quantum computer will have to do multishot QAOA. Note that any classical preprocessing for QAOA will be at least linear in time since one must read the input and produce a quantum circuit. Therefore, for small $p < 6$ QAOA will not give significant advantage: for any fast QAOA device one needs a fast classical computer; one might just run the classical FLIP algorithm on it.

The Gurobi solver is able to achieve substantially better performance, and it slightly outperforms $p = 11$ QAOA. Moreover, the BURER2002 algorithm demonstrates even better solution quality than does Gurobi while being significantly faster. For both Gurobi and BURER2002, the $\Delta_{11}(t_0) > 0$, and we need to either perform multishot QAOA or increase p . Figure 7 shows the advantage sampling frequency $\nu_{11}(t_0)$ for the Gurobi and BURER2002 algorithms; note that the vertical axis is doubly exponential.

The sampling frequency is a result of two factors that work in opposite directions. On the one hand, the time to solution for a classical algorithm grows with N , and hence ν drops. On the other hand, the variance of distribution vanishes as $1/\sqrt{N}$, and therefore the number of samples K grows exponentially. There is an optimal size N for which the sampling frequency is minimal. This analysis shows that there is a possibility for advantage with multishot QAOA for moderate sizes of $N = 100..10\,000$, for which a sampling frequency of $\approx 10\text{kHz}$ is required.

For large N , as expected, we see a rapid growth of sampling frequency, which indicates that QAOA does not scale for larger graph sizes, unless we go to higher depth $p > 11$. The color shading shows correspondence with Fig. 1. If the quantum device is able to run $p \geq 11$ and its sampling frequency and the number of qubits N corresponds to the green area, we have a quantum advantage. Otherwise, the quantum device belongs to the red area, and there is no advantage.

VI. CONCLUSION

Recently, QAOA has gained attention as a promising candidate for the demonstration of quantum advantage. However, a crucial necessity for determining quantum advantage is the evaluation of the relative performance of quantum and classical algorithms given equivalent resources. This paper evaluates a few classical algo-

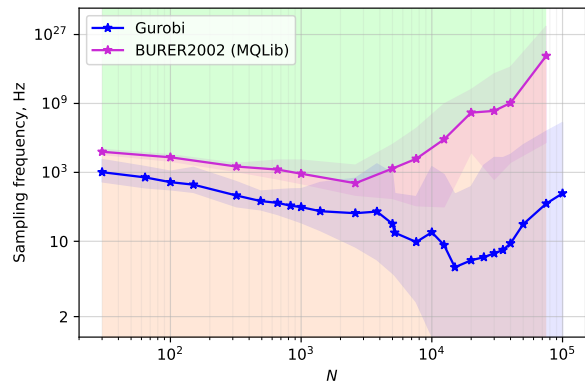


FIG. 7. Sampling frequency required to achieve MaxCut advantage using QAOA $p = 11$. The shaded area around the solid lines corresponds to 90-10 percentiles over 100 seeds for Gurobi and 20 seeds for BURER2002. The background shading represents comparison of a quantum computer with BURER2002 solver corresponding to modes in Fig. 1. Each quantum device can be represented on this plot as a point, where the x-axis is the number of qubits, and the y-axis is the time to solution. Depending on the region where the point lands, there are different results of comparisons. QAOA becomes inefficient for large N , when sampling frequency starts to grow exponentially with N .

gorithms on a subset of combinatorial optimization problems: MaxCut on 3-regular graphs, which is a widespread benchmarking problem. We show that modern classical solvers are very competitive, in terms of both solution quality and time to solution, which makes achieving quantum advantage a hard challenge.

As shown in Fig. 1, to achieve quantum advantage, QAOA must return better solutions faster than the competing classical algorithm. This puts stringent requirements on the speed of QAOA, which previously may have gone unevaluated. If QAOA returns a solution more slowly, the competing classical algorithm may “try again” to improve its solution, as is the case for anytime optimizers such as the Gurobi solver. The simplest way to improve the speed of QAOA is to reduce the number of queries to the quantum device, which we propose in our fixed-angle QAOA approach. This implementation forgoes the variational optimization step and uses solution concentration, reducing the number of samples to order 1 instead of order 100,000. Even with these improvements, however, the space of quantum advantage may be difficult to access.

Our work demonstrates that with a quantum computer of ≈ 100 qubits, QAOA can be competitive with classical MaxCut solvers if the time to solution is shorter than $100\ \mu\text{s}$ and the depth of the QAOA circuit is $p \geq 6$. However, the required speed of the quantum device grows with N exponentially. Even if an experiment shows advantage for intermediate N and $p \leq 11$, the advantage will be lost on larger problems regardless of the quantum

sampling rate. Thus, in order to be fully competitive with classical MaxCut solvers, quantum computers have to increase solution quality, for instance by using $p \geq 12$. Notably, $p = 12$ is required but not sufficient for achieving advantage: the end goal is obtaining a cut fraction better than ≥ 0.885 for large N , including overcoming other challenges of quantum devices such as noise.

These results lead us to conclude that for 3-regular graphs (perhaps all regular graphs), achieving quantum advantage on NISQ devices may be difficult. For example, the fidelity requirements to achieve quantum advantage are well above the characteristics of NISQ devices.

Compared with the MaxCut-only heuristic BURER2002, the Gurobi algorithm has similar performance on par with QAOA $p = 11$ but larger time to the first solution. It is theoretically possible to demonstrate advantage over Gurobi using smaller p with multishot QAOA, but such advantage would be possible only for small N . For full performance and speed advantage, fixed-angle QAOA must evaluate a noiseless $p \geq 11$ circuit on thousands of qubits in seconds.

We note that improved versions of QAOA exist, where the initial state is replaced with a preoptimized state [35] or the mixer operator is adapted to improve performance [36]. One also can use information from classical solvers to generate a better ansatz state [37]. These algorithms have further potential to compete against classical MaxCut algorithms. Also, more general problems, such as weighted MaxCut, maximum independent set, and 3-SAT, may be necessary in order to find problem instances suitable for achieving quantum advantage.

When comparing with classical algorithms, one must record the complete time to solution from the circuit configuration to the measured state. This parameter may be used in the extension of the notion of “quantum volume,” which is customarily used for quantum device characterization. Our work shows that QAOA MaxCut does not scale with graph size for at least up to $p \leq 11$, thus putting quantum advantage for this problem away from

the NISQ era.

VII. ACKNOWLEDGEMENTS

This material is based upon work supported by the Defense Advanced Research Projects Agency (DARPA) under Contract No. HR001120C0068. Y.A.’s and D.L.’s work at Argonne National Laboratory was supported by the U.S. Department of Energy, Office of Science, under contract DE-AC02-06CH11357. The work at UWM was also supported by the U.S. Department of Energy, Office of Science, National Quantum Information Science Research Centers.

VIII. DATA AVAILABILITY

The code, figures and datasets generated during the current study are available in a public repository <https://github.com/danlkv/quantum-classical-time-maxcut>. See the README.md file for the details on the contents of the repository. [NOTE TO NPJ EDITORS AND REVIEWERS: the repository is currently private and will remain so until this study published. We can provide the access to the private repository for reviewers upon request.]

IX. AUTHOR CONTRIBUTION

D. L. and J. W. performed and analyzed the experiments and wrote the main text. C. P. generated the FLIP data. M. S., T. N., and Y. A. edited the paper.

X. COMPETING INTERESTS

T. N. and M. S. are equity holders of and employed by ColdQuanta, a quantum technology company. J.W. is a small equity holder of and employed by QuEra Computing.

* dlykov@anl.gov
 † cpoole2@wisc.edu
 ‡ msaffman@wisc.edu
 § tom.noel@coldquanta.com
 ¶ yuri@anl.gov

¹ Yuri Alexeev, Dave Bacon, Kenneth R Brown, Robert Calderbank, Lincoln D Carr, Frederic T Chong, Brian DeMarco, Dirk Englund, Edward Farhi, Bill Fefferman, *et al.*, “Quantum computer systems for scientific discovery,” *PRX Quantum* **2**, 017001 (2021).

² Frank Arute, Kunal Arya, Ryan Babbush, Dave Bacon, Joseph C Bardin, Rami Barends, Rupak Biswas, Sergio Boixo, Fernando GSL Brandao, David A Buell, *et al.*, “Quantum supremacy using a programmable supercon-

ducting processor,” *Nature* **574**, 505–510 (2019).

³ John Preskill, “Quantum computing and the entanglement frontier,” arXiv preprint arXiv:1203.5813 (2012).

⁴ Sepehr Ebadi, Alexander Keesling, Madelyn Cain, Tout T Wang, Harry Levine, Dolev Bluvstein, Giulia Semeghini, Ahmed Omran, Jinguo Liu, Rhine Samajdar, *et al.*, “Quantum optimization of maximum independent set using rydberg atom arrays,” arXiv preprint arXiv:2202.09372 (2022).

⁵ G. G. Guerreschi and A. Y. Matsuura, “QAOA for Max-Cut requires hundreds of qubits for quantum speed-up,” *Sci. Rep.* **9**, 6903 (2019).

⁶ Leo Zhou, Sheng-Tao Wang, Soonwon Choi, Hannes Pichler, and Mikhail D. Lukin, “Quantum approximate opti-

- mization algorithm: Performance, mechanism, and implementation on near-term devices,” *Phys. Rev. X* **10**, 021067 (2020).
- 7 Michel Fabrice Serret, Bertrand Marchand, and Thomas Ayrat, “Solving optimization problems with Rydberg analog quantum computers: Realistic requirements for quantum advantage using noisy simulation and classical benchmarks,” *Phys. Rev. A* **102**, 052617 (2020).
 - 8 John Preskill, “Quantum computing in the NISQ era and beyond,” *Quantum* **2**, 79 (2018).
 - 9 M. Cerezo, Andrew Arrasmith, Ryan Babbush, Simon C. Benjamin, Suguru Endo, Keisuke Fujii, Jarrod R. McClean, Kosuke Mitarai, Xiao Yuan, Lukasz Cincio, and Patrick J. Coles, “Variational quantum algorithms,” *Nature Reviews Physics* **3**, 625–644 (2021).
 - 10 Alberto Peruzzo, Jarrod McClean, Peter Shadbolt, Man-Hong Yung, Xiao-Qi Zhou, Peter J Love, Alán Aspuru-Guzik, and Jeremy L O’Brien, “A variational eigenvalue solver on a photonic quantum processor,” *Nature communications* **5**, 1–7 (2014).
 - 11 Edward Farhi, Jeffrey Goldstone, and Sam Gutmann, “A quantum approximate optimization algorithm,” (2014), [arXiv:1411.4028 \[quant-ph\]](https://arxiv.org/abs/1411.4028).
 - 12 Sepehr Ebadi, Alexander Keesling, Madelyn Cain, Tout T. Wang, Harry Levine, Dolev Bluvstein, Giulia Semeghini, Ahmed Omran, Jinguo Liu, Rhine Samajdar, Xiu-Zhe Luo, Beatrice Nash, Xun Gao, Boaz Barak, Edward Farhi, Subir Sachdev, Nathan Gemelke, Leo Zhou, Soonwon Choi, Hannes Pichler, Shengtao Wang, Markus Greiner, Vladan Vuletic, and Mikhail D. Lukin, “Quantum optimization of maximum independent set using Rydberg atom arrays,” (2022), [10.48550/ARXIV.2202.09372](https://arxiv.org/abs/10.48550/ARXIV.2202.09372).
 - 13 Edward Farhi, David Gamarnik, and Sam Gutmann, “The quantum approximate optimization algorithm needs to see the whole graph: A typical case,” (2020), [arXiv:2004.09002 \[quant-ph\]](https://arxiv.org/abs/2004.09002).
 - 14 Turbasu Chatterjee, Shah Ishmam Mohtashim, and Akash Kundu, “On the variational perspectives to the graph isomorphism problem,” (2021).
 - 15 Ruslan Shaydulin, Ilya Safro, and Jeffrey Larson, “Multistart methods for quantum approximate optimization,” *2019 IEEE High Performance Extreme Computing Conference (HPEC)* (2019), [10.1109/hpec.2019.8916288](https://doi.org/10.1109/hpec.2019.8916288).
 - 16 Michael Streif and Martin Leib, “Training the quantum approximate optimization algorithm without access to a quantum processing unit,” (2019), [arXiv:1908.08862 \[quant-ph\]](https://arxiv.org/abs/1908.08862).
 - 17 Alexey Galda, Xiaoyuan Liu, Danylo Lykov, Yuri Alexeev, and Ilya Safro, “Transferability of optimal QAOA parameters between random graphs,” (2021), [arXiv:2106.07531 \[quant-ph\]](https://arxiv.org/abs/2106.07531).
 - 18 Jonathan Wurtz and Peter Love, “MaxCut quantum approximate optimization algorithm performance guarantees for $p > 1$,” *Phys. Rev. A* **103**, 042612 (2021).
 - 19 Jonathan Wurtz and Danylo Lykov, “The fixed angle conjecture for QAOA on regular MaxCut graphs,” (2021), [arXiv:2107.00677 \[quant-ph\]](https://arxiv.org/abs/2107.00677).
 - 20 Danylo Lykov, Roman Schutski, Alexey Galda, Valerii Vinokur, and Yuri Alexeev, “Tensor network quantum simulator with step-dependent parallelization,” *arXiv preprint arXiv:2012.02430* (2020).
 - 21 Danylo Lykov and Yuri Alexeev, “Importance of diagonal gates in tensor network simulations,” (2021), [10.48550/arXiv.2106.15740](https://arxiv.org/abs/10.48550/arXiv.2106.15740).
 - 22 Danylo Lykov, Angela Chen, Huaxuan Chen, Kristopher Keipert, Zheng Zhang, Tom Gibbs, and Yuri Alexeev, “Performance evaluation and acceleration of the QTensor quantum circuit simulator on GPUs,” *2021 IEEE/ACM Second International Workshop on Quantum Computing Software (QCS)* (2021), [10.1109/qcs54837.2021.00007](https://doi.org/10.1109/qcs54837.2021.00007).
 - 23 Eran Halperin, Dror Livnat, and Uri Zwick, “MAX CUT in cubic graphs,” **53**, 169–185 (2004).
 - 24 Michel X. Goemans and David P. Williamson, “Improved approximation algorithms for maximum cut and satisfiability problems using semidefinite programming,” *J. ACM* **42**, 1115–1145 (1995).
 - 25 LLC Gurobi Optimization, “Gurobi optimizer reference manual,” <https://www.gurobi.com> (2021).
 - 26 Iain Dunning, Swati Gupta, and John Silberholz, “What works best when? a systematic evaluation of heuristics for Max-Cut and QUBO,” **30**, 608–624 (2018).
 - 27 LLC Gurobi Optimization, “Mixed integer programming basics,” <https://www.gurobi.com/resource/mip-basics/> (2021).
 - 28 <https://support.gurobi.com/hc/en-us/community/posts/4403570181137-Worse-performance-for-smaller-problem>.
 - 29 Jonathan Wurtz and Peter J. Love, “Counterdiabaticity and the quantum approximate optimization algorithm,” (2021), [arXiv:2106.15645 \[quant-ph\]](https://arxiv.org/abs/2106.15645).
 - 30 Rebekah Herrman, Lorna Treffert, James Ostrowski, Phillip C. Lotshaw, Travis S. Humble, and George Siopsis, “Impact of graph structures for QAOA on MaxCut,” (2021), [arXiv:2102.05997 \[quant-ph\]](https://arxiv.org/abs/2102.05997).
 - 31 Ruslan Shaydulin, Kunal Marwaha, Jonathan Wurtz, and Phillip C. Lotshaw, “QAOAKit: A toolkit for reproducible study, application, and verification of the QAOA,” (2021), [arXiv:2110.05555 \[quant-ph\]](https://arxiv.org/abs/2110.05555).
 - 32 Ruslan Shaydulin and Stefan M. Wild, “Exploiting symmetry reduces the cost of training qaoa,” *IEEE Transactions on Quantum Engineering* **2**, 1–9 (2021).
 - 33 Jason Larkin, Matías Jonsson, Daniel Justice, and Gian Giacomo Guerreschi, “Evaluation of QAOA based on the approximation ratio of individual samples,” (2020), [arXiv:2006.04831 \[quant-ph\]](https://arxiv.org/abs/2006.04831).
 - 34 Matthew P. Harrigan, Kevin J. Sung, Matthew Neeley, Kevin J. Satzinger, Frank Arute, Kunal Arya, Juan Atalaya, Joseph C. Bardin, Rami Barends, Sergio Boixo, Michael Broughton, Bob B. Buckley, David A. Buell, Brian Burkett, Nicholas Bushnell, Yu Chen, Zijun Chen, Ben Chiaro, Roberto Collins, William Courtney, Sean Demura, Andrew Dunsworth, Daniel Eppens, Austin Fowler, Brooks Foxen, Craig Gidney, Marissa Giustina, Rob Graff, Steve Habegger, Alan Ho, Sabrina Hong, Trent Huang, L. B. Ioffe, Sergei V. Isakov, Evan Jeffrey, Zhang Jiang, Cody Jones, Dvir Kafri, Kostyantyn Kechedzhi, Julian Kelly, Seon Kim, Paul V. Klimov, Alexander N. Korotkov, Fedor Kostritsa, David Landhuis, Pavel Laptev, Mike Lindmark, Martin Leib, Orion Martin, John M. Martinis, Jarrod R. McClean, Matt McEwen, Anthony Megrant, Xiao Mi, Masoud Mohseni, Wojciech Mroczkiewicz, Josh Mutus, Ofer Naaman, Charles Neill, Florian Neukart, Murphy Yuezhen Niu, Thomas E. O’Brien, Bryan O’Gorman, Eric Ostby, Andre Petukhov, Harald Putterman, Chris Quintana, Pedram Roushan, Nicholas C. Rubin, Daniel Sank, Andrea Skolik, Vadim Smelyanskiy, Doug Strain, Michael Streif, Marco Szalay, Amit Vainsencher, Theodore White, Z. Jamie Yao, Ping Yeh, Adam Zalcman, Leo Zhou,

- Hartmut Neven, Dave Bacon, Erik Lucero, Edward Farhi, and Ryan Babbush, “Quantum approximate optimization of non-planar graph problems on a planar superconducting processor,” *Nature Physics* **17**, 332–336 (2021).
- ³⁵ Daniel J. Egger, Jakub Mareček, and Stefan Woerner, “Warm-starting quantum optimization,” *Quantum* **5**, 479 (2021).
- ³⁶ Linghua Zhu, Ho Lun Tang, George S. Barron, F. A. Calderon-Vargas, Nicholas J. Mayhall, Edwin Barnes, and Sophia E. Economou, “An adaptive quantum approximate optimization algorithm for solving combinatorial problems on a quantum computer,” (2020), [arXiv:2005.10258](https://arxiv.org/abs/2005.10258) [quant-ph].
- ³⁷ Jonathan Wurtz and Peter Love, “Classically optimal variational quantum algorithms,” (2021), [arXiv:2103.17065](https://arxiv.org/abs/2103.17065) [quant-ph].
- ³⁸ Thomas Häner and Damian S. Steiger, “0.5 petabyte simulation of a 45-qubit quantum circuit,” *Proceedings of the International Conference for High Performance Computing, Networking, Storage and Analysis SC '17* (2017), [10.1145/3126908.3126947](https://doi.org/10.1145/3126908.3126947).
- ³⁹ Xin-Chuan Wu, Sheng Di, Emma Maitreyee Dasgupta, Franck Cappello, Hal Finkel, Yuri Alexeev, and Frederic T. Chong, “Full-state quantum circuit simulation by using data compression,” *Proceedings of the International Conference for High Performance Computing, Networking, Storage and Analysis* (2019), [10.1145/3295500.3356155](https://doi.org/10.1145/3295500.3356155).
- ⁴⁰ Danylo Lykov, “QTensor,” <https://github.com/danlkv/Qtensor> (2021).
- ⁴¹ Henry Liu, Junyu Liu, Rui Liu, Henry Makhanov, Danylo Lykov, Anuj Apte, and Yuri Alexeev, “Embedding learning in hybrid quantum-classical neural networks,” (2022).
- ⁴² Rina Dechter, “Bucket elimination: A unifying framework for several probabilistic inference,” *CoRR abs/1302.3572* (2013), [arXiv:1302.3572](https://arxiv.org/abs/1302.3572).
- ⁴³ Daniel J Harvey and David R Wood, “The treewidth of line graphs,” *Journal of Combinatorial Theory, Series B* **132**, 157–179 (2018).
- ⁴⁴ Igor L Markov and Yaoyun Shi, “Simulating quantum computation by contracting tensor networks,” *SIAM Journal on Computing* **38**, 963–981 (2008).
- ⁴⁵ Roman Schutski, Danil Lykov, and Ivan Oseledets, “Adaptive algorithm for quantum circuit simulation,” *Phys. Rev. A* **101**, 042335 (2020).
- ⁴⁶ Johnnie Gray and Stefanos Kourtis, “Hyper-optimized tensor network contraction,” *Quantum* **5**, 410 (2021).
- ⁴⁷ Juneseo Lee, Alicia B. Magann, Herschel A. Rabitz, and Christian Arenz, “Progress toward favorable landscapes in quantum combinatorial optimization,” *Phys. Rev. A* **104**, 032401 (2021).
- ⁴⁸ Robert Elsässer and Tobias Tscheuschner, “Settling the complexity of local Max-Cut (almost) completely,” in *Automata, Languages and Programming*, edited by Luca Aceto, Monika Henzinger, and Jiří Sgall (Springer Berlin Heidelberg, Berlin, Heidelberg, 2011) pp. 171–182.
- ⁴⁹ Ahmed El Alaoui, Andrea Montanari, and Mark Sellke, “Local algorithms for maximum cut and minimum bisection on locally treelike regular graphs of large degree,” (2021), [arXiv:2111.06813](https://arxiv.org/abs/2111.06813) [math.PR].
- ⁵⁰ Boaz Barak and Kunal Marwaha, “Classical algorithms and quantum limitations for maximum cut on high-girth graphs,” (2021), [arXiv:2106.05900](https://arxiv.org/abs/2106.05900) [quant-ph].
- ⁵¹ Nicholas C. Wormald, “The asymptotic distribution of short cycles in random regular graphs,” *Journal of Combinatorial Theory, Series B* **31**, 168–182 (1981).
- ⁵² Brendan D. McKay, Nicholas C. Wormald, and Beata Wysocka, “Short cycles in random regular graphs,” *The Electronic Journal of Combinatorics* **11**, R66 (2004).

Appendix A: Quantum simulator QTensor

The most popular method for quantum circuit simulation is state-vector evolution. It stores full state vector and hence requires memory size $\propto 2^N$, exponential in the number of qubits. It can simulate only circuits with $\lesssim 30$ qubits on a common computer, and simulation of 45 qubits on a supercomputer was reported [38]. One can perform compression of the state vector and therefore simulate up to 61 qubits on a supercomputer [39].

For this work, we aim to study performance of QAOA on instances large enough to use in comparison with classical solvers. To simulate expectation values on large graphs, we use the classical simulator QTensor [20; 40]. This simulator is based on tensor network contraction and allows for simulation of a much larger number of qubits. QTensor converts a quantum circuit to a tensor network, where each quantum gate is represented by a tensor. The indices of this tensor represent input and output subspaces of each qubit that the gate acts on. The tensor network constructed in this way can then be contracted in an efficient manner to compute the required value. The contraction does not maintain any information about the structure of the original quantum circuit, and can result in significant simulation cost reduction, not limited to the QAOA context [41].

To calculate an expectation value of some observable \hat{R} in a state generated by a circuit \hat{U} , one can evaluate the following expression: $\langle 0 | \hat{U}^\dagger \hat{R} \hat{U} | 0 \rangle$. This value can be calculated by using a tensor network as well. When applied to the MaxCut QAOA problem, the \hat{R} operator is a sum of smaller terms, as shown in Eq. 2. The expectation value of the cost for the graph G and QAOA depth p is then

$$\begin{aligned} \langle C \rangle_p(\vec{\gamma}, \vec{\beta}) &= \langle \vec{\gamma}, \vec{\beta} | \hat{C} | \vec{\gamma}, \vec{\beta} \rangle \\ &= \sum_{\langle jk \rangle \in G} \langle \vec{\gamma}, \vec{\beta} | \frac{1}{2} (1 - \hat{\sigma}_z^j \hat{\sigma}_z^k) | \vec{\gamma}, \vec{\beta} \rangle \\ &= \sum_{\langle jk \rangle \in G} f_{\langle jk \rangle}(\vec{\gamma}, \vec{\beta}), \end{aligned}$$

where $f_{\langle jk \rangle} = \langle \vec{\gamma}, \vec{\beta} | (1 - \hat{\sigma}_z^j \hat{\sigma}_z^k) | \vec{\gamma}, \vec{\beta} \rangle / 2$ is an individual edge contribution to the total cost function. Each contribution to the cost function $f_{\langle jk \rangle}$ can be evaluated by using a corresponding tensor network. Note that the observable $\hat{\sigma}_z^j \hat{\sigma}_z^k$ in the definition of $f_{\langle jk \rangle}$ acts only on two qubits and hence commutes with gates that act on other qubits. The $\langle \vec{\gamma}, \vec{\beta} |$ state is not stored in memory at any time but rather is represented as a tensor network generated from the quantum circuit shown in Eq. 1. When

two such tensor network representations (one for $\langle \vec{\gamma}, \vec{\beta} \rangle$ and another for $|\vec{\gamma}, \vec{\beta}\rangle$) are joined aside of the observable operator, it is possible to cancel out the quantum gates that commute through the observable, thereby significantly reducing the size of the tensor network. The tensor network after the cancellation is equivalent to calculating $\hat{\sigma}_z^j \hat{\sigma}_z^k$ on a subgraph S of the original graph G .

While multiple approaches exist for determining the best way to contract a tensor network, we use a contraction approach called bucket elimination [42], which contracts one index at a time. At each step we choose some index j from the tensor expression and then sum over a product of tensors that have j in their index. The size of the intermediary tensor obtained as a result of this operation is very sensitive to the order in which indices are contracted. To find a good contraction ordering, we use a line graph of the tensor network. A tree decomposition [43] of the line graph corresponds to a contraction path that guarantees that the number of indices in the largest intermediary tensor will be equal to the width of the tree decomposition [44]. In this way one can simulate QAOA to reasonable depth on hundreds or thousands of qubits. More details of QTENSOR and tensor networks are in [20; 45; 46].

Appendix B: FLIP

As an example of a simple and fast classical MaxCut algorithm we evaluate a local search algorithm. This class of heuristic is frequently referred to as FLIP [47] or FLIP-neighborhood [48]. A FLIP algorithm heuristic searches locally for improvements to the current solution that flip a single vertex. One still retains the freedom to choose how to search for the vertex to flip at each stage of the algorithm. Examples of vertex selection methods include randomized message passing [49] and zero temperature annealing.

The FLIP algorithm is as follows. First, for each vertex of a graph, initially assign a value of 0 or 1 at random with equal probability. From this starting point, randomly order the vertices of the graph, iterate through each vertex in order, and flip the vertex if flipping it will improve the cut value. Once all vertices have been iterated through, repeat this process until no vertices are changed in a full iteration. This procedure is analogous to zero-temperature Monte Carlo annealing and is a greedy solver. The end result is a partition in which flipping any individual vertex will not improve the cut size. On 3-regular graphs we observe that this algorithm runs on graphs of $N = 10,000$ nodes in about 70 ms on an Intel I9-10900K processor and gives a mean cut fraction of 0.847, which matches the performance of $p = 6$ QAOA.

Given more time, the FLIP algorithm can improve its performance by reinitializing with a new random choice of vertex assignments and vertex orderings, as shown in Fig. 4. Given an exponential number of repetitions, the algorithm will eventually converge on the exact result,

p	1	2	3	4	5	6
f_{Tree}	0.6925	0.7559	0.7924	0.8169	0.8364	0.8499
f_3	0.6369	0.6457	0.6561	0.6594	0.6594	0.6618
f_4		0.7905	0.8606	0.8980	0.9315	0.9486
f_5		0.7503	0.7684	0.7842	0.7876	0.7911
f_6			0.7971	0.8248	0.8580	0.8813
f_7			0.7919	0.8160	0.8297	0.8361
f_8				0.8169	0.8376	0.8546
f_9				0.8169	0.8363	0.8489
f_{10}					0.8364	0.8500
f_{11}					0.8364	0.8499
f_{12}						0.8499
f_{13}						0.8499

TABLE I. Expectation values of subgraphs. Columns index depth of QAOA, while rows index subgraphs. The first row is the expectation value of the tree subgraph, while subsequent rows are subgraphs that participate in a single cycle of size d . We note that the value for large cycles is close to the tree value, suggesting that longer range QAOA does not get much extra advantage to distinguish between different values.

although very slowly.

As a local binary algorithm, it runs into locality restrictions [50] and less-than-ideal performance but is extremely fast. To put this into perspective with QAOA, we implemented FLIP using Python. We observe that a simple implementation returns solutions for a 100,000 vertex 3-regular graph in < 1 second. Optimized or parallelized implementation using high-performance languages such as C++ may run several times faster. The main property is that for a graph of degree k , girth L , and size N , the FLIP algorithm runtime scales as $O(NLk)$ [49], which we verify experimentally. Notably, for any quantum initialisation step the time scaling would also be at least $O(N)$, since we have to somehow move information about the graph to the quantum device.

Appendix C: Graph statistics bounds

It is known [51; 52] that in the limit $N \rightarrow \infty$, the probability of a graph having t cycles of length l , where connectivity d is odd, is asymptotic to

$$P(l, t) = \frac{\lambda^t \exp(-\lambda)}{t!} \quad \text{where} \quad \lambda = \frac{(d-1)^l}{2l}. \quad (\text{C1})$$

Summing over all t , we find that the average number of cycles of size l is equal to the same size-independent constant

$$m_l = \sum_{t=0}^{\infty} tP(l, t) = \frac{(d-1)^l}{2l}. \quad (\text{C2})$$

This is a probabilistic estimate based on statistics of regular graphs, does not depend on QAOA, and is asymptotically precise; thus, this is a “with high probability”

(WHP) result. We use this count to bound the number of each kind of subgraph. Given a d -regular graph of N vertices, there are $M = dN/2$ edges. The maximum number of edges that participate in a cycle of length l happens when each edge from such cycle participates only in one cycle of length l . With high probability at most lm_l edges participate in a cycle of length l . By extension, the center edge of a tree subgraph participates in no cycles $\leq 2p + 1$, and so the number of tree subgraphs is with high probability at least

$$M_{\text{p-tree}} \geq M - \sum_{l=3}^{2p+1} lm_l. \quad (\text{C3})$$

Note that $M_{\text{p-tree}}$ should trivially be ≥ 0 , which occurs for large p and small N .

The expectation value as a sum over subgraphs can then be broken into two parts: the tree subgraph and everything else. This can then be bounded by fixing an extremal value for the expectation value of every other subgraph, knowing that $0 \leq f_\lambda \leq 1$.

$$\langle \hat{C} \rangle = M_{\text{p-tree}} f_{\text{tree}} + \sum_{\lambda \neq \text{p-tree}} M_\lambda f_\lambda, \quad (\text{C4})$$

$$\leq M - M_{\text{p-tree}}(1 - f_{\text{p-tree}}), \quad (\text{C5})$$

$$\geq M_{\text{p-tree}} f_{\text{p-tree}} \quad (\text{C6})$$

Therefore, for N large, the value of $\langle \hat{C} \rangle$ is bounded from above and below by a constant amount and converges to the tree value. Similarly, for N small, the value of $\langle \hat{C} \rangle$ is bounded between 0 and 1 as WHP every edge participates in at least one cycle of length $l \leq 2p + 1$ and so there are no tree subgraphs to contribute to the count.

These bounds may be tightened by including expectation values f_λ for more subgraphs. The next most common subgraph is that having a single cycle of length $l = 2p + 1$ and participating in no other cycles. The number of such subgraphs is then bounded from below by

$$M_{l\text{-cycle}} \geq lm_l \left(1 - \frac{M_{\text{p-tree}}}{M}\right). \quad (\text{C7})$$

The expectation value is then bounded by

$$\begin{aligned} \langle \hat{C} \rangle &\leq M - M_{\text{p-tree}}(1 - f_{\text{tree}}) - \sum_{l=3}^{2p+1} M_{l\text{-cycle}}(1 - f_{l\text{-cycle}}), \\ &\geq M_{\text{p-tree}} f_{\text{tree}} + \sum_{l=3}^{2p+1} M_{l\text{-cycle}} f_{l\text{-cycle}}. \end{aligned} \quad (\text{C8})$$

In principle, this may be done indefinitely, by including more and more subgraphs.

Using Table I for evaluations of single-loop subgraphs at fixed angles, we may evaluate Eq. (C8) to bound the cut fraction $\langle \hat{C} \rangle / M$ as a function of the graph size N , as is shown in Fig. 2. This is a “with high probability” result: there may be extremely atypical graphs that have much different numbers of tree and single cycle subgraphs. For example, an atypical graph may be one of size N that is two graphs of size $N/2$ connected by a single edge. This bound is a generalization of the work of [13], which observes that the QAOA needs to “see the whole graph” in order to have advantage. Here the upper and lower bounds are based on the same argument, except generalized to the small- N regime and including more subgraphs to tighten the bounds.